Examining the Effect of an Anion-Binding Reagent on the Structure of Deprotonated Leucine Enkephalin Using Cryogenic-Ion Infrared Action Spectroscopy

*Madeline Schultz,[†] Nwanne D. Banor,[†] Katja Ober,[‡] America Y. Torres-Boy, [‡] Maleesha T. Fernando,[†] Miyuru M. Wellalage,[†] Neil A. Ellis,[†] Gert von Helden,[‡] Daniel A. Thomas[†,]**

[†]Department of Chemistry, University of Rhode Island, Kingston, RI 02881, USA

[‡]Fritz-Haber-Institut der Max-Planck Gesellschaft, Faradayweg 4-6, 14195 Berlin, Germany

*dathomas@uri.edu

Abstract

Biomolecular systems feature a complex interaction network comprising numerous intra- and intermolecular interactions. By isolating biomolecules under vacuum conditions, the intricate balance between specific interaction motifs can be characterized with precise control over conditions. In this study, we apply cryogenic-ion infrared action spectroscopy and electronic structure methods to examine the structural changes in the deprotonated form of the model peptide leucine enkephalin (YGGFL) upon complexation with diserinol isophthalamide (DIP), an anion-binding reagent. The low-energy conformer of the uncomplexed, deprotonated peptide ($[YGGFL - H]^-$) adopts a noncanonical turn structure stabilized by intramolecular ionic hydrogen bonding to the C-terminal carboxylate moiety. Despite the favorability of DIP to strongly coordinate with carboxylate residues, we find that the structure of the peptide is largely unaffected by the binding of DIP. Instead, DIP only partially coordinates with the carboxylate moiety and is positioned below the backbone turn of YGGFL to engage in additional hydrogen bonding interactions. These findings underscore the stability of the turn structure and the strong energetic penalty imposed by disruption of this motif even when strong intermolecular coordination is expected.

Introduction

Biomolecular secondary, tertiary, and quaternary structures are stabilized by a network of inter- and intramolecular interactions. The subtle balance between these structural motifs governs system behavior across protein-water,[1-4] protein-protein,[5-7] and protein-ligand interactions.[8-12] A precise description of these interactions is especially relevant for elucidating the structure and evolution of highly dynamic systems, such as intrinsically disordered proteins and biomolecules undergoing liquid-liquid phase separation.[9-15] However, the inherent complexity of these interactions in the condensed phase presents a significant experimental challenge.[3, 9] Mass spectrometry (MS) and related techniques have emerged as a powerful tool for the analysis of biological structure that complements traditional condensed-phase studies.[16-20] Prominent techniques include hydrogen-deuterium exchange (HDX) MS for the comparative analysis of structure and dynamics,[16, 21-23] ultraviolet photodissociation (UVPD) or electron-based dissociation (ExD) for the identification of structure and noncovalent interactions,[17, 24-30] ion mobility spectrometry (IMS) for the elucidation of three-dimensional structure,[19, 31-35] and action spectroscopy for the systematic analysis of isolated conformers.[20, 36-39] For small biological molecules such as peptides, infrared action spectroscopy can be leveraged to reveal the noncovalent interaction network and analyze the contribution of each interaction to higher-order structure.[37, 40-42]

This work is concerned with changes in the peptide conformational landscape upon binding of a small molecule to charged sites. By contrast between bound and unbound conformations, these systems reveal the structural stabilization provided by intramolecular ionic hydrogen bonding. Previously, the model pentapeptide leucine enkephalin (YGGFL) has served as a test case for such studies. The unbound, protonated form of YGGFL has been widely characterized by structure-sensitive techniques including infrared multiple-photon dissociation (IRMPD),[43] ultraviolet photodissociation (UVPD),[44] ion mobility spectrometry (IMS),[34, 45] and infrared-ultraviolet (IR-UV) double resonance photofragment spectroscopy.[41] It is known to adopt a type II' β-turn with prominent ionic hydrogen bonds to the protonated N-terminus.[46, 47] To investigate the contribution of charge-site interactions to the stability of the turn structure, the complex between protonated YGGFL and 18-crown-6 was previously examined by cryogenic-ion infrared (IR) action spectroscopy.[48] 18-crown-6 is known to bind monoalkylammonium residues via intermolecular hydrogen bonding,[48-58] thereby disrupting the intramolecular interactions between the N-terminus and the backbone carbonyl groups. Complexation was observed to result in reorientation of the protonated N-terminus, but surprisingly, the overall β-turn structure of the peptide was preserved.[48]

Scheme 1. Structure of diserinol isophthalamide (DIP) and leucine enkephalin (YGGFL).

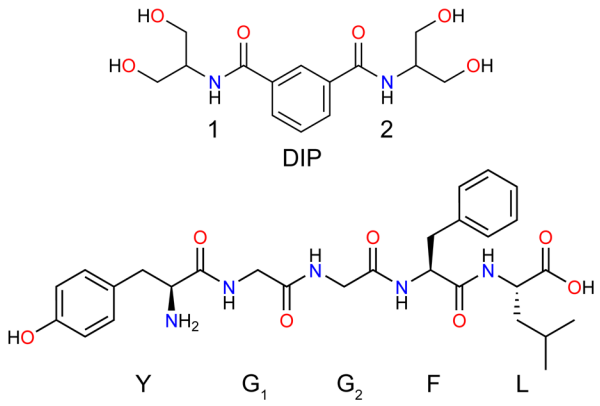

Herein, we examine the contribution of ionic hydrogen bonding to the structure of deprotonated YGGFL[59] by complexing the peptide with an anion-binding reagent, diserinol isophthalamide[60] (DIP, Scheme 1), which binds carboxylate moieties of biomolecular ions during the electrospray process.[60, 61] Similar to studies on the protonated form of YGGFL, structural characterization of both the bound and unbound conformers provides information on the importance of intramolecular interactions of the carboxylate residue. The uncomplexed, deprotonated form of YGGFL has previously been characterized by IR action spectroscopy and IMS.[62] As with protonated YGGFL, the low-energy conformer of the deprotonated molecule adopts a turn structure with multiple ionic hydrogen bonds to the charge site, in this case the C-terminal carboxylate group. However, the bond angles indicate a noncanonical turn structure rather than the type II' β-turn observed for the protonated form. In this work, we investigate whether this turn structure is preserved upon complexation of the peptide with DIP, which is expected to compete for ionic hydrogen bond interactions with the carboxylate moiety.

To characterize the structure of deprotonated YGGFL and its complex with DIP, ions are prepared by electrospray ionization mass spectrometry (ESI–MS) and captured in helium

nanodroplets for IR action spectroscopy. This approach has been applied extensively for the characterization of biomolecular ion structure.[48, 63-68] Nanodroplet-entrained ions are cooled to 0.4 K, resulting in population of only low-energy states and enabling acquisition of highly resolved IR spectra. Ion photon absorption results in evaporation of He atoms and ultimately generation of the bare ion. Monitoring ion yield as a function of photon wavelength yields an IR action spectrum. The experimental spectra are compared to predicted conformer spectra obtained from electronic structure methods to identify the peptide structure.

Methods

Experimental Methods

Infrared action spectroscopy of ions in helium nanodroplets was performed using custom instrumentation described previously (Figure S1).[67-69] Briefly, ions were generated by nanoelectrospray ionization (nESI) from Pd/Pt-coated pulled-glass needles prepared in-house. Ions were mass-to-charge (*m*/*z*) selected by a quadrupole mass filter, bent 90° by a quadrupole deflector, and loaded into a hexapole ion trap held at ca. 90 K. A beam of helium nanodroplets, generated by a pulsed Even-Lavie valve[70] at a pressure of ca. 70 bar and a temperature of 21 K,[68] traversed the ion trap, resulting in ion capture. Ion-doped droplets escaped the trap and traveled to a ring-electrode ion guide, wherein they were irradiated with IR photons generated by the free-electron laser (FEL) at the Fritz Haber Institute.[71] FEL pulses were ca. 10 μs in length and composed of ca. 10^4 ps-length micropulses at a repetition rate of 1 GHz.[67] Energy from the absorption of resonant photons was dissipated via intramolecular and intermolecular vibrational redistribution, ultimately causing He evaporation. The successive absorption of photons from individual FEL micropulses resulted in nanodroplet evaporation and the generation of bare ions,[72] which were detected by an off-axis time-of-flight (TOF) detector.

The intensity at a given photon energy was obtained as the integrated target *m*/*z* ion signal from the average of 25 FEL macropulses. Measurements were collected between 1250 and 1750 cm^{-1} in 1 cm^{-1} steps, and the ion trap was refilled between each measurement step. Laser power was adjusted depending on line intensity to achieve operation in a pseudo-linear response regime,[72] and combined spectra were scaled by the intensity of lines overlapping between scans. Intensities were corrected for photon fluence by scaling with a factor of (laser power × wavenumber)$^{-1}$. Each region was scanned at least twice and averaged to ensure reproducibility.

Sample solutions were prepared from leucine enkephalin salt hydrate (purity ≥95%, Merck Millipore, Darmstadt, Germany) and diserinol isophthalamide (DIP), which was synthesized as described previously.[60] To prepare sample solutions, YGGFL was dissolved in 50/50 H_2O/MeOH (v/v%), and DIP was dissolved in H_2O. From 1 mM stock solutions, samples were then diluted in 50/50 H_2O/MeOH (v/v%). YGGFL was prepared at a final concentration of 150 μM. For study of the complexed species, a solution was prepared at concentrations of 500 μM DIP and 50 μM YGGFL.

Conformational Sampling via CREST

Conformational sampling was performed for deprotonated YGGFL ($[YGGFL - H]^-$), the complex between YGGFL and DIP ($[YGGFL + DIP - H]^-$), and the complex between acetate and DIP ($[CH_3OO^- + DIP]^-$) using the conformer-rotamer ensemble sampling tool (CREST)

developed by Pracht, Grimme, and co-workers, wherein low-energy conformers are identified using metadynamic simulations with semi-empirical extended tight-binding (xTB) methods.[73-75] Sampling was performed at the GFN2-xTB level of theory[76] with the default energy window of 25 kJ mol^{-1} for [YGGFL – H]$^-$ (carboxylate and phenolate deprotomers), [YGGFL + DIP – H]$^-$ (carboxylate, phenolate, and DIP alkoxide deprotomers), and [CH_3OO^- + DIP]$^-$. An additional search for [YGGFL + DIP – H]$^-$ in the carboxylate form was performed using the non-covalent interactions (nci) run-type, which generates an ellipsoidal potential to encapsulate non-covalently bound species during the metadynamic simulations and disfavor dissociation.[77] The ellipsoidal potential wall was scaled by a factor of two. Further conformational sampling for [YGGFL + DIP – H]$^-$ (carboxylate, phenolate, and alkoxide deprotomers) was performed using the LEDE-CREST variant designed for noncovalent clusters.[78]

Geometry Optimization and Frequency Calculations via ORCA

For the carboxylate deprotomers, all structures obtained from CREST were optimized within the ORCA software package[79, 80] using the B3LYP hybrid density functional with the D3BJ empirical dispersion correction[81-84] and the def2-TZVP basis set.[85-87] Unless otherwise noted, the RIJCOSX approximation[88] was used with the def2/J auxiliary basis set.[89] Low-energy conformers were additionally optimized using the long-range parametrized CAM-B3LYP(D3BJ) hybrid density functional[90] and ωB97X-D3 hybrid density functional[91] with the def2-TZVP basis set. Separately, the CAM-B3LYP(D3BJ)/def2-TZVP level of theory was used for optimization of phenolate and deprotonated DIP conformers obtained from CREST. Finally, conformers obtained from LEDE-CREST were manually screened using the *measure cluster* feature of VMD,[92] and unique conformers were optimized at the CAM-B3LYP(D3BJ)/def2-TZVP level of theory.

For the lowest-energy conformer of [YGGFL – H]$^-$, B3LYP(D3BJ) optimization was also performed with the ma-def2-SVP,[85, 93] ma-def2-TZVP,[93] and def2-TZVPP basis sets.[85] The auxiliary basis set aug-cc-pVTZ/JK[94] was used with the minimally augmented basis sets, ma-def2-SVP and ma-def2-TZVP. Additionally, the lowest-energy conformer was optimized with the PBE0 hybrid density functional[95, 96] and D3BJ dispersion correction[86, 87] with the ma-def2-SVP, ma-def2-TZVP, def2-TZVP, and def2-TZVPP basis sets. Harmonic vibrational normal mode frequencies were calculated for all low-energy structures using analytic second derivatives of the Born-Oppenheimer potential. Frequencies were convoluted with Gaussian distributions with a full width at half maximum of 0.3% (in wavenumber) centered at each frequency and scaled by best fit to experimental spectra using Pearson and Spearman correlation coefficients,[97] with scaling factors ranging from 0.96-0.99.

Results and Discussion

Spectroscopy and Conformational Analysis of Deprotonated YGGFL

Shown in Figure 1a is the IR action spectrum of deprotonated YGGFL, [YGGFL – H]$^-$, in the fingerprint region. Notably, the He nanodroplet technique enables resolution of lines in the range of 1640 to 1700 cm^{-1}, where three partially resolved lines are attributed to amide I modes (a_6–a_8), and one line is assigned to the carboxylate asymmetric stretch (a_5). Four amide I bands are expected, one for each amide bond in the peptide, but the shoulder visible for line a_6 and the broadening of line a_7 may indicate the population of multiple conformers.

Lines attributable to the amide II modes (a_2–a_4) are also observed, with line a_4 noticeably shifted with respect to other amide II bands. A diffuse feature, line a_1, is found in the region of amide III, carboxylate symmetric stretching, and CH bending modes.

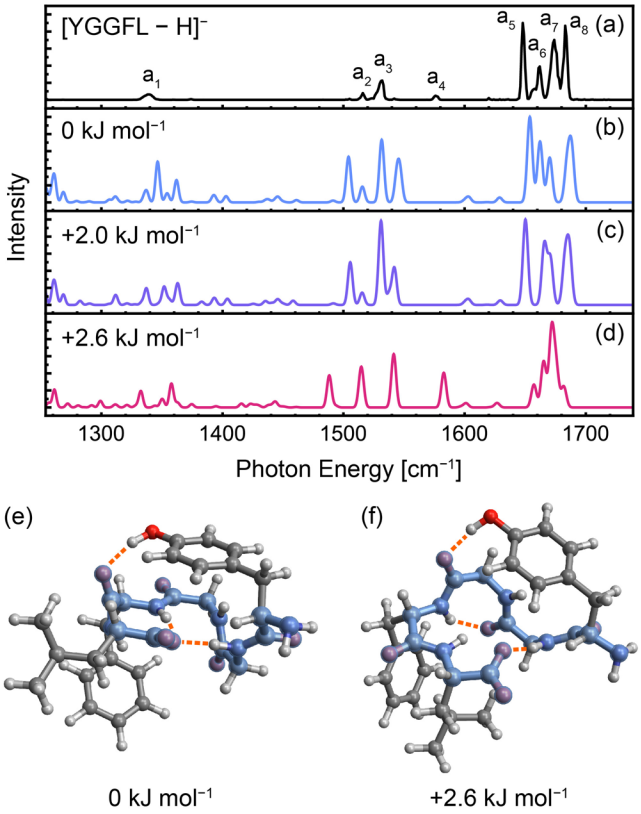

Figure 1. Infrared action spectrum of $[YGGFL-H]^-$ captured in helium nanodroplets (a) and computed spectra for the three lowest-energy [Δ(*E*+*ZPE*)] conformers (b–d) at the CAM-B3LYP(D3BJ)/def2-TZVP level of theory (0.96 scaling factor). The structure of the lowest- and third-lowest energy conformers are shown in (e) and (f), respectively, with the backbone highlighted in blue. The five lowest-energy structures are shown in Figure S2.

The low-energy conformers of YGGFL were identified by conformational sampling with the GFN2-xtb semi-empirical method within CREST and subsequent geometry optimization and vibrational frequency calculation using various density functionals and basis sets. A comparison of basis sets with the B3LYP(D3BJ) and PBE0(D3BJ) density functionals showed large changes when progressing from ma-def2-SVP to def2-TZVP but only minor changes between def2-TZVP and def2-TZVPP or ma-def2-TZVP (Figures S6 and S7). Therefore, the def2-TZVP basis set was chosen for further calculations as a balance between accuracy and computational cost. In comparing density functionals, little difference in the relative energy of conformers was observed (Tables S3 and S4). For IR spectra, a Spearman and Pearson coefficient analysis was applied to find the best agreement between experiment and theory and optimize the scaling factors.[97] The best agreement with the experimental spectrum of $[YGGFL - H]^-$ was found using the CAM-B3LYP(D3BJ)/def2-TZVP level of theory with a scaling factor of 0.96, and this approach was used for all further analysis. A comparison of spectra obtained from various density functionals is shown in Figure S9.

Shown in Figures 1b–d are the spectra of the identified low-energy conformers of [YGGFL – H]$^-$ computed at the CAM-B3LYP(D3BJ)/def2-TZVP level of theory. The lowest-energy conformer (Figure 1e, spectrum Figure 1b) comprises a turn structure featuring two hydrogen bonds to the C-terminal carboxylate and a hydrogen bond between the Tyr side chain and Phe backbone carbonyl (see Figure S5 for a schematic depiction of hydrogen bonds). The second-lowest-energy structure (+2.0 kJ mol^{-1} after zero-point energy (*ZPE*) correction) differs only in the orientation of the Leu side chain (spectrum in Figure 1c). Both structures belong to the family of lowest-energy conformers previously reported by Schinle *et al*,[62] which exhibit a noncanonical turn structure (Ramachandran angles provided in Table S6). The slightly higher-energy conformer shown in Figure 1f exhibits a similar backbone structure with a slightly altered hydrogen bonding pattern. The amide nitrogen of the second glycine residue (Gly_2) forms a hydrogen bond with an adjacent carbonyl group rather than the C-terminus, and the hydrogen bond of the tyrosine side chain is shifted from the Phe carbonyl to the Gly_2 carbonyl. In addition, the phenylalanine and leucine side chains are reoriented to facilitate a CH–π interaction. Higher-energy conformers within 10 kJ mol^{-1} of the identified minimum-energy structure were found to have similar backbone configurations and hydrogen bonding patterns to those shown in Figures 1e, f, as illustrated in Figure S2. The lowest-energy phenolate structure was found to be 23.0 kJ mol^{-1} higher in energy (Figure S4, Table S3) and belongs to the family of structures previously reported.[62] The computed IR spectrum of this deprotomer shows poor agreement with experiment (Figure S10). Therefore, although previous studies of isolated hydroxybenzoic and coumaric acids have demonstrated an energetic preference for the phenolate deprotomer, this property is not observed for the larger YGGFL system.

Good agreement is observed between the experimental spectrum (Figure 1a) and the predicted spectra of the two lowest-energy conformers (Figures 1b, c). The spectrum of the higher-energy conformer (Figure 1d) exhibits poorer overall agreement, but the match with line a_4, assigned to a blue-shifted amide II mode, is notable. In addition, the blue-shift of the carboxylate asymmetric stretching mode, arising from loss of hydrogen-bonding interactions with the C-terminus, and corresponding shifts of amide I modes may explain the shoulder of line a_6 and broadening of line a_7. Thus, the experimental spectrum is consistent with the population of all three conformers. The relative intensity of line a_4 would suggest a relative population of ca. 10% for the +2.6 kJ mol^{-1} conformer, whereas a Boltzmann population at the trap temperature of 90 K would give a population of ca. 3% (assuming kinetic trapping of conformer population upon capture in He nanodroplets).[98-100] This discrepancy may arise from the inaccuracy of the applied electronic structure methods or the trapping of population during ion cooling within the trap.[101] In addition, the non-linear response inherent to the He nanodroplet method may lead to an incorrect estimation of relative population based on line intensities.[54]

Spectroscopy and Conformational Analysis of the YGGFL + DIP Complex

Figure 2b displays the IR action spectrum of the complex between deprotonated YGGFL and DIP, [YGGFL + DIP – H]$^-$. The spectrum of [YGGFL – H]$^-$ is shown in Figure 2a for reference. Upon complexation to DIP, a substantial red-shift of ca. 50 cm^{-1} is observed for the line assigned to the carboxylate asymmetric stretching band (line b_6 vs line a_5). In addition, the distribution of lines in the amide I region is compressed, with two closely spaced

but broad amide I bands between 1660 and 1690 cm^{-1} (lines b_7 and b_8). The carboxylate symmetric stretch (line b_2) is noticeably blue-shifted from the corresponding line for the unbound species (line a_1). A new line of moderate intensity is observed at 1276 cm^{-1} (b_1), in the range of CH and NH bending modes. The strong shift of the lines corresponding to carboxylate symmetric and asymmetric stretching is indicative of the formation of new hydrogen-bonding interactions with the deprotonated C-terminus. Note that DIP introduces new features in the fingerprint region, most notably those arising from the amide modes of this molecule.

Initial conformational sampling of the deprotonated YGGFL+DIP complex was performed with the GFN2-xtb semi-empirical method within CREST using default settings. Additional sampling was performed with the LEDE-CREST approach, which is designed to sample the potential energy surface of flexible noncovalent complexes. Structures were subsequently optimized using DFT methods. For the carboxylate deprotomers, similar low-energy structures were found by the two methods, whereas lower-energy phenolate deprotomers were identified by CREST, and lower-energy alkoxide deprotomers were found by LEDE-CREST. All low-energy carboxylate structures (<10 kJ mol^{-1} ΔE+*ZPE*, Table S4) were found to adopt a similar peptide backbone configuration, with variation found largely in the orientation of the Leu and Phe side chains and in the hydrogen bonding interactions of the serinol moiety of DIP not coordinated with the carboxylate group, as depicted in Figure S3. Phenolate or DIP deprotomers were found to be substantially higher in energy (+68.4 and +86.2 kJ mol^{-1} ΔE+*ZPE*, Table S4).

The lowest-energy complex between YGGFL and DIP (Figure 2h) is characterized by two new hydrogen bonds to the carboxylate moiety as well as two new hydrogen bonds to the peptide backbone, one to the N-terminus and one to the Gly_1 carbonyl (see Figure S5). Comparing the minimum-energy structure of unbound YGGFL (Figure 1e) to that of the YGGFL + DIP complex (Figure 2h), the hydrogen-bonding configuration of the peptide is preserved, with two hydrogen bonds coordinated to the C-terminus and one hydrogen bond between the Tyr side chain and Phe backbone carbonyl. Overall, the YGGFL structure within the low-energy DIP complex is largely unchanged as compared to the unbound species.

The predicted IR spectra of low-energy conformers of deprotonated $[YGGFL + DIP - H]^-$ are displayed in Figures 2c–g, and the structure of the lowest-energy conformer is shown in Figure 2h. Phenolate and alkoxide deprotomers yielded a poor match with the experimental IR spectrum (Figure S11). In comparing the experimental and theoretical IR spectra, discussion here is limited to the minimum-energy structure shown in Figure 2h and corresponding IR spectrum in Figure 2c, as other low-energy conformers adopt a similar structure and exhibit comparable line positions. The amide I bands in Figure 2c are clustered into two groups, which can be divided between hydrogen-bonded amide I (line c_7) and free amide I (line c_8) modes. Note that these lines arise from amide I modes of both YGGFL and DIP. This grouping is largely consistent with that observed experimentally (lines b_7 and b_8), but the predicted lines are much broader and more widely spaced. Line c_6, arising from the carboxylate asymmetric stretching mode, is slightly blue-shifted with respect to the corresponding experimental line b_6. The most intense lines arising from amide II modes, c_4 and c_5, also exhibit small shifts in intensity and position from the experimental lines b_4 and b_5. Notably, the normal modes associated with these bands involve multiple amide bonds or coupling with side-chain deformation modes, rendering the line positions and intensities

sensitive to small structural perturbations (compare Figures 2c–g). Line c_3 corresponds to CH_2 scissoring modes and is red-shifted from the assigned experimental line b_3. Finally, line c_2 arises from the carboxylate symmetric stretch coupled with CH bending modes, and line c_1 encompasses several weak CH and NH bending modes.

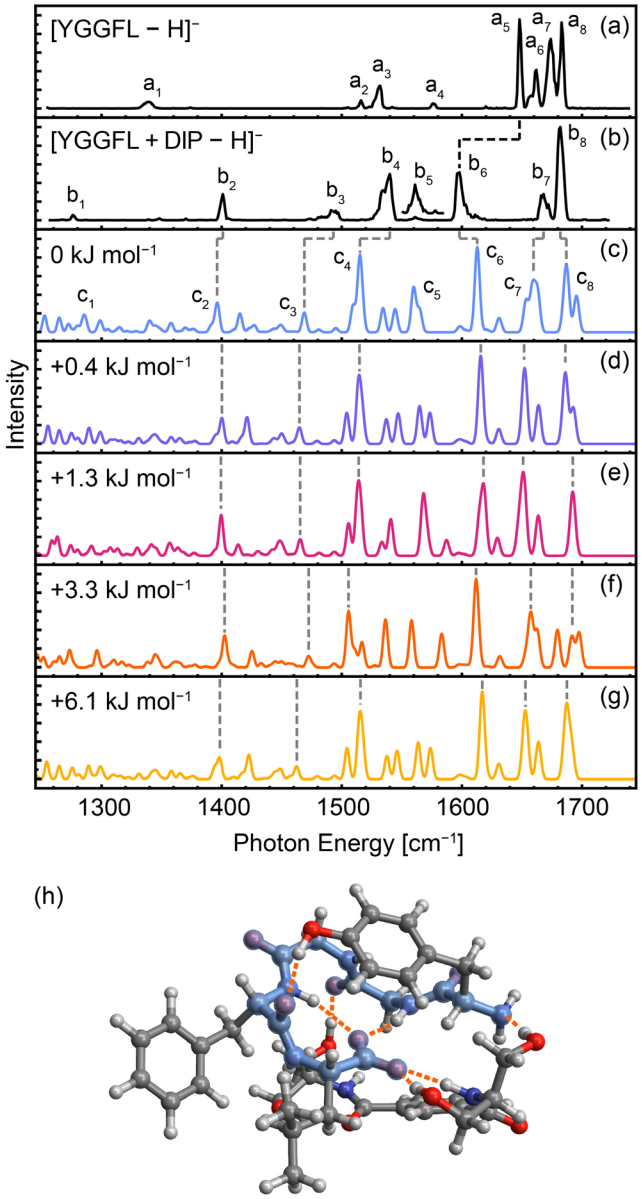

Figure 2. Infrared action spectrum of $[YGGFL-H]^-$ (a) and $[YGGFL + DIP - H]^-$ (b) captured in helium nanodroplets and computed spectra for the five lowest-energy [Δ(E+ZPE)] conformers of $[YGGFL + DIP - H]^-$ (c–g) at the CAM-B3LYP(D3BJ)/def2-TZVP level of theory (0.96 scaling factor). The structure of the lowest-energy conformer is shown in (h), with the peptide backbone highlighted in blue. Line b_5 in (b) is shown with a magnification factor of ten.

Agreement between experimental and theoretical IR spectra is notably poorer for the YGGFL + DIP complex than for the unbound peptide. The increased complexity of the

noncovalent interactions between YGGFL and DIP may introduce vibrational anharmonicities that partially account for this deviation. However, the agreement between experiment and theory is sufficient to support assignment of the experimental spectrum to the predicted low-energy structure. Although DIP complexation is expected to favor formation of a strongly hydrogen-bonded pocket around the carboxylate moiety,[60] the structural disruption required to achieve such a binding motif imposes a significant enthalpic penalty. No low-energy structure was identified that featured full coordination of DIP with the C-terminus and favorable intramolecular interactions of YGGFL. Instead, DIP binds to deprotonated YGGFL by alignment below the turn structure, with one serinol moiety coordinating to the carboxylate and one forming a hydrogen bond with a backbone carbonyl. Notably, the low-energy structures of the phenolate and DIP deprotomers do not feature a peptide turn structure, exhibiting instead a pseudo-linear peptide arrangement (Figure S4). These arrangements result in significantly reduced backbone hydrogen bonding, contributing to the substantial enthalpic penalty for these deprotomers as compared to the turn-preserving carboxylate structure (+68.4 and +86.2 kJ mol^{-1} ΔE+*ZPE*).

Conformational Sampling of the DIP + Acetate Complex

To better understand the changes in the DIP binding motif imposed by complexation with YGGFL, the conformation of DIP in [YGGFL + DIP – H]$^-$ was compared to that in the acetate complex, [CH_3OO^- + DIP]$^-$. Note that the low-energy structure of [CH_3OO^- + DIP]$^-$ discussed here differs from that previously reported[60] owing to a more extensive conformational sampling protocol. As shown in Figure 3a, the [CH_3OO^- + DIP]$^-$ complex features symmetric intramolecular hydrogen bonds between a hydroxyl group and each amide carbonyl moiety. The acetate anion is located in a binding pocket formed by the remaining four hydrogen bond donors, two serinol OH and two amide NH groups. As shown in Figure 3b, the structural constraints necessary to preserve the turn structure of YGGFL substantially alter this optimized hydrogen bonding network. For [YGGFL + DIP – H]$^-$, only one serinol moiety of DIP is coordinated to the carboxylate group, and the orientation of the remaining serinol group is inverted with respect to the aromatic ring to avoid steric clashes with the peptide backbone. This orientation also favors a hydrogen bond to a backbone carbonyl rather than coordination with the carboxylate group. A hydroxyl group on the carboxylate-coordinated serinol also forms a hydrogen bond with the N-terminus rather than an intramolecular hydrogen bond with the amide carbonyl, although this interaction results in only a minor change in the coordination with the charge site. Overall, although the full coordination of the charge site with DIP is favored in the absence of steric constraints, the stability of the turn structure of YGGFL is sufficient to dictate a reduced coordination in the low-energy structure of [YGGFL + DIP – H]$^-$. It is notable that the number of hydrogen bonds to the charge site is comparable, although the length and angles of these interactions reduce the overall strength. The flexibility of the DIP hydrogen-bond donors also contributes to the propensity of this reagent to bind with alternate orientations.

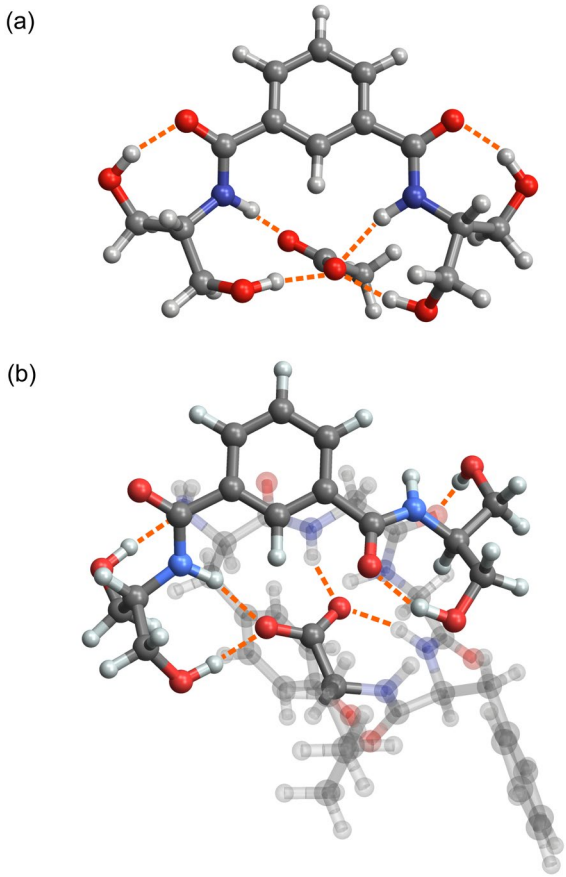

Figure 3. Comparison of the binding motif of the complex between DIP and acetate, $[CH_3OO^- + DIP]^-$ (a), and the complex between DIP and deprotonated YGGFL, $[YGGFL + DIP - H]^-$ (b). Atoms of YGGFL other than the C-terminus are displayed as translucent for clarity. The structural constraints imposed by interaction with YGGFL substantially alter the observed hydrogen-bonding network with the charge site. Structures were optimized at the CAM-B3LYP(D3BJ)/def2-TZVP level of theory.

Conclusion

The structure adopted by biomolecules arises from the balance of intermolecular and intramolecular interactions. Herein, we have investigated changes in the molecular structure of a model peptide upon complexation with an anion-binding reagent. Using cryogenic IR action spectroscopy, we have confirmed the noncanonical turn structure of deprotonated YGGFL, supported by both backbone hydrogen bonding and ionic hydrogen bonding to the C-terminal carboxylate. Perhaps surprisingly, it was found that this structure was largely preserved upon binding of DIP to the peptide, despite the preference of this reagent to encompass carboxylate residues. This result points to the unique stability of the observed turn structure, which is not easily replicated by alternate conformations that could better facilitate DIP coordination at the C-terminus. A similar result was obtained previously for the complex between protonated YGGFL and 18-crown-6, wherein charge site hydrogen bonding was more extensively disrupted while preserving the general backbone conformation.[48] In addition, the preservation of structure upon capping of a C-terminal hydrogen bond donor in

protonated YGGFL was also reported.[47] Together, these results point to the robustness of peptide backbone structure against perturbations at the chain termini.

AUTHOR INFORMATION

Corresponding Author

*Daniel A. Thomas- Department of Chemistry, University of Rhode Island, Kingston, Rhode Island 02881, United States Email: dathomas@uri.edu

Author Contributions

The manuscript was written through contributions of all authors. All authors have given approval to the final version of the manuscript.

ASSOCIATED CONTENT

The following files are available free of charge.

Schematic of instrumentation, depiction of low-energy conformers, basis set dependence of vibrational frequency calculations, vibrational spectra of low-energy conformers, tabulation of experimental lines, relative energies of electronic structure methods, results of CREST sampling, peptide Ramachandran angles (PDF)

XYZ coordinates from electronic structure calculations, experimental IR action spectra (TXT)

ACKNOWLEDGMENT

The authors are grateful to Dr. Wieland Schöllkopf and Sandy Gewinner for support in the use and operation of the free-electron laser at the Fritz-Haber-Institut der Max-Planck-Gesellschaft. This work was supported by startup funding from the University of Rhode Island and NSF grant CHE-2212926.

ABBREVIATIONS

DIP, diserinol isophthalamide; ESI-MS, electrospray ionization mass spectrometry; nESI, nano electrospray; FEL, free-electron laser; TOF, time-of-flight.

REFERENCES

(1) Qin, Y.; Wang, L.; Zhong, D. Dynamics and mechanism of ultrafast water–protein interactions. *Proc. Nat. Acad. Sci. U.S.A.* **2016**, *113* (30), 8424-8429. DOI: 10.1073/pnas.1602916113.

(2) Chun, S. Y.; Son, M. K.; Park, C. R.; Lim, C.; Kim, H. I.; Kwak, K.; Cho, M. Direct observation of protein structural transitions through entire amyloid aggregation processes in water using 2D-IR spectroscopy. *Chem. Sci.* **2022**, *13* (16), 4482-4489. DOI: 10.1039/D1SC06047C.

(3) Hunt, N. T. Using 2D-IR Spectroscopy to Measure the Structure, Dynamics, and Intermolecular Interactions of Proteins in H_2O. *Acc. Chem. Res.* **2024**, *57* (5), 685-692. DOI: 10.1021/acs.accounts.3c00682.

(4) Son, M. K.; Im, D.; Hyun, D. G.; Kim, S.; Chun, S. Y.; Choi, J.-M.; Choi, T. S.; Cho, M.; Kwak, K.; Kim, H. I. Accelerated Amyloid Aggregation Dynamics of Intrinsically Disordered Proteins in Heavy Water. *J. Phys. Chem. Lett.* **2024**, *15* (47), 11823-11829. DOI: 10.1021/acs.jpclett.4c02764.

(5) Milroy, L.-G.; Grossmann, T. N.; Hennig, S.; Brunsveld, L.; Ottmann, C. Modulators of Protein–Protein Interactions. *Chem. Rev.* **2014**, *114* (9), 4695-4748. DOI: 10.1021/cr400698c.

(6) Watanabe, H.; Yoshida, C.; Ooishi, A.; Nakai, Y.; Ueda, M.; Isobe, Y.; Honda, S. Histidine-Mediated Intramolecular Electrostatic Repulsion for Controlling pH-Dependent Protein–Protein Interaction. *ACS Chem. Biol.* **2019**, *14* (12), 2729-2736. DOI: 10.1021/acschembio.9b00652.

(7) Monteleone, S.; Fedorov, D. G.; Townsend-Nicholson, A.; Southey, M.; Bodkin, M.; Heifetz, A. Hotspot Identification and Drug Design of Protein–Protein Interaction Modulators Using the Fragment Molecular Orbital Method. *J. Chem. Inf. Model.* **2022**, *62* (16), 3784-3799. DOI: 10.1021/acs.jcim.2c00457.

(8) Hudson, B. M.; Nguyen, E.; Tantillo, D. J. The influence of intramolecular sulfur–lone pair interactions on small-molecule drug design and receptor binding. *Org. Biomol. Chem.* **2016**, *14* (16), 3975-3980. DOI: 10.1039/C6OB00254D.

(9) Ban, D.; Iconaru, L. I.; Ramanathan, A.; Zuo, J.; Kriwacki, R. W. A Small Molecule Causes a Population Shift in the Conformational Landscape of an Intrinsically Disordered Protein. *J. Am. Chem. Soc.* **2017**, *139* (39), 13692-13700. DOI: 10.1021/jacs.7b01380.

(10) Herrera-Nieto, P.; Pérez, A.; De Fabritiis, G. Small Molecule Modulation of Intrinsically Disordered Proteins Using Molecular Dynamics Simulations. *J. Chem. Inf. Model.* **2020**, *60* (10), 5003-5010. DOI: 10.1021/acs.jcim.0c00381.

(11) Robustelli, P.; Ibanez-de-Opakua, A.; Campbell-Bezat, C.; Giordanetto, F.; Becker, S.; Zweckstetter, M.; Pan, A. C.; Shaw, D. E. Molecular Basis of Small-Molecule Binding to α-Synuclein. *J. Am. Chem. Soc.* **2022**, *144* (6), 2501-2510. DOI: 10.1021/jacs.1c07591.

(12) Heller, G. T.; Shukla, V. K.; Figueiredo, A. M.; Hansen, D. F. Picosecond Dynamics of a Small Molecule in Its Bound State with an Intrinsically Disordered Protein. *J. Am. Chem. Soc.* **2024**, *146* (4), 2319-2324. DOI: 10.1021/jacs.3c11614.

(13) Paloni, M.; Bailly, R.; Ciandrini, L.; Barducci, A. Unraveling Molecular Interactions in Liquid–Liquid Phase Separation of Disordered Proteins by Atomistic Simulations. *J. Phys. Chem. B* **2020**, *124* (41), 9009-9016. DOI: 10.1021/acs.jpcb.0c06288.

(14) Guo, Q.; Zou, G.; Qian, X.; Chen, S.; Gao, H.; Yu, J. Hydrogen-bonds mediate liquid-liquid phase separation of mussel derived adhesive peptides. *Nat. Commun.* **2022**, *13* (1), 5771. DOI: 10.1038/s41467-022-33545-w.

(15) König, B.; Pezzotti, S.; Ramos, S.; Schwaab, G.; Havenith, M. Real-time measure of solvation free energy changes upon liquid-liquid phase separation of α-elastin. *Biophys. J.* **2024**, *123* (11), 1367-1375. DOI: 10.1016/j.bpj.2023.07.023.

(16) Konermann, L.; Vahidi, S.; Sowole, M. A. Mass Spectrometry Methods for Studying Structure and Dynamics of Biological Macromolecules. *Anal. Chem.* **2014**, *86* (1), 213-232. DOI: 10.1021/ac4039306.

(17) Liu, R.; Xia, S.; Li, H. Native top-down mass spectrometry for higher-order structural characterization of proteins and complexes. *Mass Spectrom. Rev.* **2023**, *42* (5), 1876-1926. DOI: 10.1002/mas.21793.

(18) Britt, H. M.; Cragnolini, T.; Thalassinos, K. Integration of Mass Spectrometry Data for Structural Biology. *Chem. Rev.* **2022**, *122* (8), 7952-7986. DOI: 10.1021/acs.chemrev.1c00356.

(19) Christofi, E.; Barran, P. Ion Mobility Mass Spectrometry (IM-MS) for Structural Biology: Insights Gained by Measuring Mass, Charge, and Collision Cross Section. *Chem. Rev.* **2023**, *123* (6), 2902-2949. DOI: 10.1021/acs.chemrev.2c00600.

(20) Rijs, A. M.; Oomens, J. IR Spectroscopic Techniques to Study Isolated Biomolecules. In *Gas-Phase IR Spectroscopy and Structure of Biological Molecules*; Rijs, A. M., Oomens, J., Eds.; Springer, 2015; pp 1-42. DOI: 10.1007/128_2014_621.

(21) Engen, J. R.; Botzanowski, T.; Peterle, D.; Georgescauld, F.; Wales, T. E. Developments in Hydrogen/Deuterium Exchange Mass Spectrometry. *Anal. Chem.* **2021**, *93* (1), 567-582. DOI: 10.1021/acs.analchem.0c04281.

(22) James, E. I.; Murphree, T. A.; Vorauer, C.; Engen, J. R.; Guttman, M. Advances in Hydrogen/Deuterium Exchange Mass Spectrometry and the Pursuit of Challenging Biological Systems. *Chem. Rev.* **2022**, *122* (8), 7562-7623. DOI: 10.1021/acs.chemrev.1c00279.

(23) Konermann, L.; Scrosati, P. M. Hydrogen/Deuterium Exchange Mass Spectrometry: Fundamentals, Limitations, and Opportunities. *Mol. Cell. Proteomics* **2024**, *23* (11). DOI: 10.1016/j.mcpro.2024.100853.

(24) Warnke, S.; Baldauf, C.; Bowers, M. T.; Pagel, K.; von Helden, G. Photodissociation of Conformer-Selected Ubiquitin Ions Reveals Site-Specific Cis/Trans Isomerization of Proline Peptide Bonds. *J. Am. Chem. Soc.* **2014**, *136* (29), 10308-10314. DOI: 10.1021/ja502994b.

(25) O'Brien, J. P.; Li, W.; Zhang, Y.; Brodbelt, J. S. Characterization of Native Protein Complexes Using Ultraviolet Photodissociation Mass Spectrometry. *J. Am. Chem. Soc.* **2014**, *136* (37), 12920-12928. DOI: 10.1021/ja505217w.

(26) Breuker, K.; McLafferty, F. W. Native Electron Capture Dissociation for the Structural Characterization of Noncovalent Interactions in Native Cytochrome c. *Angew. Chem., Int. Ed.* **2003**, *42* (40), 4900-4904. DOI: 10.1002/anie.200351705.

(27) Xie, Y.; Zhang, J.; Yin, S.; Loo, J. A. Top-Down ESI-ECD-FT-ICR Mass Spectrometry Localizes Noncovalent Protein-Ligand Binding Sites. *J. Am. Chem. Soc.* **2006**, *128* (45), 14432-14433. DOI: 10.1021/ja063197p.

(28) Li, H.; Wolff, J. J.; Van Orden, S. L.; Loo, J. A. Native Top-Down Electrospray Ionization-Mass Spectrometry of 158 kDa Protein Complex by High-Resolution Fourier Transform Ion Cyclotron Resonance Mass Spectrometry. *Anal. Chem.* **2014**, *86* (1), 317-320. DOI: 10.1021/ac4033214.

(29) Lermyte, F.; Konijnenberg, A.; Williams, J. P.; Brown, J. M.; Valkenborg, D.; Sobott, F. ETD Allows for Native Surface Mapping of a 150 kDa Noncovalent Complex on a Commercial Q-TWIMS-TOF Instrument. *J. Am. Soc. Mass Spectrom.* **2014**, *25* (3), 343-350. DOI: 10.1007/s13361-013-0798-3.

(30) Li, H.; Nguyen, H. H.; Ogorzalek Loo, R. R.; Campuzano, I. D. G.; Loo, J. A. An integrated native mass spectrometry and top-down proteomics method that connects sequence to

structure and function of macromolecular complexes. *Nat. Chem.* **2018**, *10* (2), 139-148. DOI: 10.1038/nchem.2908.

(31) Konijnenberg, A.; Butterer, A.; Sobott, F. Native ion mobility-mass spectrometry and related methods in structural biology. *Biochim. Biophys. Acta, Proteins Proteomics* **2013**, *1834* (6), 1239-1256. DOI: 10.1016/j.bbapap.2012.11.013.

(32) Gabelica, V.; Marklund, E. Fundamentals of ion mobility spectrometry. *Curr. Opin. Chem. Biol.* **2018**, *42*, 51-59. DOI: 10.1016/j.cbpa.2017.10.022.

(33) Wyttenbach, T.; Pierson, N. A.; Clemmer, D. E.; Bowers, M. T. Ion Mobility Analysis of Molecular Dynamics. *Annu. Rev. Phys. Chem.* **2014**, *65* (1), 175-196. DOI: 10.1146/annurev-physchem-040513-103644.

(34) Bleiholder, C.; Dupuis, N. F.; Wyttenbach, T.; Bowers, M. T. Ion mobility–mass spectrometry reveals a conformational conversion from random assembly to β-sheet in amyloid fibril formation. *Nat. Chem.* **2011**, *3* (2), 172-177. DOI: 10.1038/nchem.945.

(35) Warnke, S.; von Helden, G.; Pagel, K. Protein Structure in the Gas Phase: The Influence of Side-Chain Microsolvation. *J. Am. Chem. Soc.* **2013**, *135* (4), 1177-1180. DOI: 10.1021/ja308528d.

(36) Wolk, A. B.; Leavitt, C. M.; Garand, E.; Johnson, M. A. Cryogenic Ion Chemistry and Spectroscopy. *Acc. Chem. Res.* **2014**, *47* (1), 202-210. DOI: 10.1021/ar400125a.

(37) Rizzo, T. R.; Boyarkin, O. V. Cryogenic Methods for the Spectroscopy of Large, Biomolecular Ions. In *Gas-Phase IR Spectroscopy and Structure of Biological Molecules*; Rijs, M. A., Oomens, J., Eds.; Springer, 2015; pp 43-97. DOI: 10.1007/128_2014_579.

(38) Kamrath, M. Z.; Rizzo, T. R. Combining Ion Mobility and Cryogenic Spectroscopy for Structural and Analytical Studies of Biomolecular Ions. *Acc. Chem. Res.* **2018**, *51* (6), 1487-1495. DOI: 10.1021/acs.accounts.8b00133.

(39) Boyarkin, O. V. Cold ion spectroscopy for structural identifications of biomolecules. *Int. Rev. Phys. Chem.* **2018**, *37* (3-4), 559-606. DOI: 10.1080/0144235X.2018.1547453.

(40) Baldauf, C.; Rossi, M. Going Clean: Structure and Dynamics of Peptides in the Gas Phase and Paths to Solvation. *J. Phys.: Condens. Matter* **2015**, *27* (49), 493002. DOI: 10.1088/0953-8984/27/49/493002.

(41) Wassermann, T. N.; Boyarkin, O. V.; Paizs, B.; Rizzo, T. R. Conformation-Specific Spectroscopy of Peptide Fragment Ions in a Low-Temperature Ion Trap. *J. Am. Soc. Mass Spectrom.* **2012**, *23* (6), 1029-1045. DOI: 10.1007/s13361-012-0368-0.

(42) Rizzo, T. R.; Stearns, J. A.; Boyarkin, O. V. Spectroscopic studies of cold, gas-phase biomolecular ions. *Int. Rev. Phys. Chem.* **2009**, *28* (3), 481-515. DOI: 10.1080/01442350903069931.

(43) Harrilal, C. P.; DeBlase, A. F.; McLuckey, S. A.; Zwier, T. S. Two-Color IRMPD Applied to Conformationally Complex Ions: Probing Cold Ion Structure and Hot Ion Unfolding. *J. Phys. Chem. A* **2021**, *125* (42), 9394-9404. DOI: 10.1021/acs.jpca.1c08388.

(44) Herburger, A.; van der Linde, C.; Beyer, M. K. Photodissociation spectroscopy of protonated leucine enkephalin. *Phys. Chem. Chem. Phys.* **2017**, *19* (17), 10786-10795. DOI: 10.1039/C6CP08436B.

(45) Polfer, N. C.; Bohrer, B. C.; Plasencia, M. D.; Paizs, B.; Clemmer, D. E. On the Dynamics of Fragment Isomerization in Collision-Induced Dissociation of Peptides. *J. Phys. Chem. A* **2008**, *112* (6), 1286-1293. DOI: 10.1021/jp0763937.

(46) Burke, N. L.; Redwine, J. G.; Dean, J. C.; McLuckey, S. A.; Zwier, T. S. UV and IR spectroscopy of cold protonated leucine enkephalin. *Int. J. Mass Spectrom.* **2015**, *378*, 196-205. DOI: 10.1016/j.ijms.2014.08.012.

(47) Burke, N. L.; DeBlase, A. F.; Redwine, J. G.; Hopkins, J. R.; McLuckey, S. A.; Zwier, T. S. Gas-Phase Folding of a Prototypical Protonated Pentapeptide: Spectroscopic Evidence for Formation of a Charge-Stabilized β-Hairpin. *J. Am. Chem. Soc.* **2016**, *138* (8), 2849-2857. DOI: 10.1021/jacs.6b00093.

(48) González Flórez, A. I.; Ahn, D.-S.; Gewinner, S.; Schöllkopf, W.; von Helden, G. IR Spectroscopy of Protonated Leu-enkephalin and its 18-crown-6 Complex Embedded in Helium Droplets. *Phys. Chem. Chem. Phys.* **2015**, *17*, 21902-21911. DOI: 10.1039/C5CP02172C.

(49) Julian, R. R.; Beauchamp, J. L. Site specific sequestering and stabilization of charge in peptides by supramolecular adduct formation with 18-crown-6 ether by way of electrospray ionization. *Int. J. Mass Spectrom.* **2001**, *210-211*, 613-623. DOI: 10.1016/S1387-3806(01)00431-6.

(50) McNary, C. P.; Nei, Y. W.; Maitre, P.; Rodgers, M. T.; Armentrout, P. B. Infrared multiple photon dissociation action spectroscopy of protonated glycine, histidine, lysine, and arginine complexed with 18-crown-6 ether. *Phys. Chem. Chem. Phys.* **2019**, *21* (23), 12625-12639. DOI: 10.1039/C9CP02265A.

(51) Liu, Z.; Cheng, S.; Gallie, D. R.; Julian, R. R. Exploring the Mechanism of Selective Noncovalent Adduct Protein Probing Mass Spectrometry Utilizing Site-Directed Mutagenesis To Examine Ubiquitin. *Anal. Chem.* **2008**, *80* (10), 3846-3852. DOI: 10.1021/ac800176u.

(52) Chen, Y.; Rodgers, M. T. Structural and Energetic Effects in the Molecular Recognition of Protonated Peptidomimetic Bases by 18-Crown-6. *J. Am. Chem. Soc.* **2012**, *134* (4), 2313-2324. DOI: 10.1021/ja2102345.

(53) Ko, J. Y.; Heo, S. W.; Lee, J. H.; Oh, H. B.; Kim, H.; Kim, H. I. Host–Guest Chemistry in the Gas Phase: Complex Formation with 18-Crown-6 Enhances Helicity of Alanine-Based Peptides. *J. Phys. Chem. A* **2011**, *115* (49), 14215-14220. DOI: 10.1021/jp208045a.

(54) Oh, Y.-H.; Oh, H. B.; Lee, S. Structural connectivity of 18-Crown-6/H+/L-tryptophan noncovalent complexes in gas phase and in solution: Delineating host–guest–solvent interactions in solution from gas phase structures. *Int. J. Quantum Chem.* **2024**, *124* (1), e27337. DOI: 10.1002/qua.27337.

(55) Ly, T.; Julian, R. R. Using ESI-MS to probe protein structure by site-specific noncovalent attachment of 18-crown-6. *J. Am. Soc. Mass Spectrom.* **2006**, *17* (9), 1209-1215. DOI: 10.1016/j.jasms.2006.05.007.

(56) Tao, Y.; Julian, R. R. Investigation of peptide microsolvation in the gas phase by radical directed dissociation mass spectrometry. *Int. J. Mass Spectrom.* **2016**, *409*, 81-86. DOI: 10.1016/j.ijms.2016.10.001.

(57) Tao, Y.; Julian, R. R. Factors that Influence Competitive Intermolecular Solvation of Protonated Groups in Peptides and Proteins in the Gas Phase. *J. Am. Soc. Mass Spectrom.* **2013**, *24* (11), 1634-1640. DOI: 10.1007/s13361-013-0684-z.

(58) Stedwell, C. N.; Galindo, J. F.; Gulyuz, K.; Roitberg, A. E.; Polfer, N. C. Crown Complexation of Protonated Amino Acids: Influence on IRMPD Spectra. *J. Phys. Chem. A* **2013**, *117* (6), 1181-1188. DOI: 10.1021/jp305263b.

(59) Sztáray, J.; Memboeuf, A.; Drahos, L.; Vékey, K. Leucine enkephalin—A mass spectrometry standard. *Mass Spectrom. Rev.* **2011**, *30* (2), 298-320. DOI: 10.1002/mas.20279.

(60) Schultz, M.; Parker, S. L.; Fernando, M. T.; Wellalage, M. M.; Thomas, D. A. Diserinol Isophthalamide: A Novel Reagent for Complexation with Biomolecular Anions in Electrospray Ionization Mass Spectrometry. *J. Am. Soc. Mass Spectrom.* **2023**, *34* (4), 745-753. DOI: 10.1021/jasms.3c00010.

(61) Schultz, M.; Ellis, N. A.; Banor, N. D.; Thomas, D. A. Complexation of diserinol isophthalamide with phosphorylated biomolecules in electrospray ionization mass spectrometry. *Int. J. Mass Spectrom.* **2025**, *507*, 117364. DOI: 10.1016/j.ijms.2024.117364.

(62) Schinle, F.; Jacob, C. R.; Wolk, A. B.; Greisch, J.-F.; Vonderach, M.; Weis, P.; Hampe, O.; Johnson, M. A.; Kappes, M. M. Ion Mobility Spectrometry, Infrared Dissociation Spectroscopy, and ab Initio Computations toward Structural Characterization of the Deprotonated Leucine-Enkephalin Peptide Anion in the Gas Phase. *J. Phys. Chem. A* **2014**, *118* (37), 8453-8463. DOI: 10.1021/jp501772d.

(63) Mucha, E.; González Flórez, A. I.; Marianski, M.; Thomas, D. A.; Hoffmann, W.; Struwe, W. B.; Hahm, H. S.; Gewinner, S.; Schöllkopf, W.; Seeberger, P. H.; et al. Glycan Fingerprinting via Cold-Ion Infrared Spectroscopy. *Angew. Chem., Int. Ed.* **2017**, *56*, 11248-11251. DOI: 10.1002/anie.201702896.

(64) Greis, K.; Kirschbaum, C.; von Helden, G.; Pagel, K. Gas-phase infrared spectroscopy of glycans and glycoconjugates. *Curr. Opin. Struct. Biol.* **2022**, *72*, 194-202. DOI: 10.1016/j.sbi.2021.11.006.

(65) González Flórez, A. I.; Mucha, E.; Ahn, D.-S.; Gewinner, S.; Schöllkopf, W.; Pagel, K.; von Helden, G. Charge-Induced Unzipping of Isolated Proteins to a Defined Secondary Structure. *Angew. Chem., Int. Ed.* **2016**, *55* (10), 3295–3299. DOI: 10.1002/anie.201510983.

(66) Mucha, E.; Marianski, M.; Xu, F.-F.; Thomas, D. A.; Meijer, G.; von Helden, G.; Seeberger, P. H.; Pagel, K. Unravelling the Structure of Glycosyl Cations via Cold-Ion Infrared Spectroscopy. *Nat. Commun.* **2018**, *9* (1), 4174. DOI: 10.1038/s41467-018-06764-3.

(67) Mucha, E. Vibrational Spectroscopy of Glycans in Helium Nanodroplets. Ph.D. Thesis, Radboud University Nijmegen, Nijmegen, 2020. https://hdl.handle.net/2066/215031.

(68) González Flórez, A. I. Biomolecular Ions in Superfluid Helium Nanodroplets. Ph.D. Thesis, Freie Universität Berlin, Berlin, 2016. https://doi.org/10.17169/refubium-10853.

(69) Filsinger, F.; Ahn, D.-S.; Meijer, G.; von Helden, G. Photoexcitation of Mass/Charge Selected Hemin$^+$, Caught in Helium Nanodroplets. *Phys. Chem. Chem. Phys.* **2012**, *14* (38), 13370-13377. DOI: 10.1039/C2CP42071F.

(70) Pentlehner, D.; Riechers, R.; Dick, B.; Slenczka, A.; Even, U.; Lavie, N.; Brown, R.; Luria, K. Rapidly pulsed helium droplet source. *Rev. Sci. Instrum.* **2009**, *80* (4). DOI: 10.1063/1.3117196 (acccessed 7/16/2025).

(71) Schöllkopf, W.; Gewinner, S.; Junkes, H.; Paarmann, A.; von Helden, G.; Bluem, H.; Todd, A. M. M. The new IR and THz FEL Facility at the Fritz Haber Institute in Berlin. *Proc. SPIE* **2015**, *9512*, 95121L. DOI: 10.1117/12.2182284.

(72) Mucha, E.; Thomas, D.; Lettow, M.; Meijer, G.; Pagel, K.; von Helden, G. Spectroscopy of Small and Large Biomolecular Ions in Helium-Nanodroplets. In *Molecules in Superfluid Helium Nanodroplets: Spectroscopy, Structure, and Dynamics*; Slenczka, A., Toennies, J. P., Eds.; Springer International Publishing, 2022; pp 241-280. DOI: 10.1007/978-3-030-94896-2_6.

(73) Pracht, P.; Grimme, S.; Bannwarth, C.; Bohle, F.; Ehlert, S.; Feldmann, G.; Gorges, J.; Müller, M.; Neudecker, T.; Plett, C.; et al. CREST—A program for the exploration of low-energy molecular chemical space. *J. Chem. Phys.* **2024**, *160* (11). DOI: 10.1063/5.0197592.

(74) Grimme, S. Exploration of Chemical Compound, Conformer, and Reaction Space with Meta-Dynamics Simulations Based on Tight-Binding Quantum Chemical Calculations. *J. Chem. Theory Comput.* **2019**, *15* (5), 2847-2862. DOI: 10.1021/acs.jctc.9b00143.

(75) Pracht, P.; Grimme, S. Calculation of absolute molecular entropies and heat capacities made simple. *Chem. Sci.* **2021**, *12* (19), 6551-6568. DOI: 10.1039/D1SC00621E.

(76) Bannwarth, C.; Ehlert, S.; Grimme, S. GFN2-xTB—An Accurate and Broadly Parametrized Self-Consistent Tight-Binding Quantum Chemical Method with Multipole Electrostatics and Density-Dependent Dispersion Contributions. *J. Chem. Theory Comput.* **2019**, *15* (3), 1652-1671. DOI: 10.1021/acs.jctc.8b01176.

(77) Grimme, S.; Bohle, F.; Hansen, A.; Pracht, P.; Spicher, S.; Stahn, M. Efficient Quantum Chemical Calculation of Structure Ensembles and Free Energies for Nonrigid Molecules. *J. Phys. Chem. A* **2021**, *125* (19), 4039-4054. DOI: 10.1021/acs.jpca.1c00971.

(78) King, N. J.; LeBlanc, I. D.; Brown, A. A variant on the CREST iMTD algorithm for noncovalent clusters of flexible molecules. *J. Comp. Chem.* **2024**, *45* (29), 2431-2445. DOI: 10.1002/jcc.27458.

(79) Neese, F. Software update: The ORCA program system—Version 5.0. *WIREs Comput. Mol. Sci.* **2022**, *12* (5), e1606. DOI: 10.1002/wcms.1606.

(80) Neese, F. The ORCA program system. *WIREs Comput. Mol. Sci.* **2012**, *2* (1), 73-78. DOI: 10.1002/wcms.81.

(81) Becke, A. D. A new mixing of Hartree–Fock and local density-functional theories. *J. Chem. Phys.* **1993**, *98* (2), 1372-1377. DOI: 10.1063/1.464304.

(82) Lee, C.; Yang, W.; Parr, R. G. Development of the Colle-Salvetti Correlation-Energy Formula into a Functional of the Electron Density. *Phys. Rev. B.* **1988**, *37* (2), 785-789. DOI: 10.1103/PhysRevB.37.785.

(83) Vosko, S. H.; Wilk, L.; Nusair, M. Accurate spin-dependent electron liquid correlation energies for local spin density calculations: a critical analysis. *Can. J. of Phys.* **1980**, *58* (8), 1200-1211. DOI: 10.1139/p80-159.

(84) Stephens, P. J.; Devlin, F. J.; Chabalowski, C. F.; Frisch, M. J. Ab Initio Calculation of Vibrational Absorption and Circular Dichroism Spectra Using Density Functional Force Fields. *J. Phys. Chem.* **1994**, *98* (45), 11623-11627. DOI: 10.1021/j100096a001.

(85) Weigend, F.; Ahlrichs, R. Balanced Basis Sets of Split Valence, Triple Zeta Valence and Quadruple Zeta Valence Quality for H to Rn: Design and Assessment of Accuracy. *Phys. Chem. Chem. Phys.* **2005**, *7* (18), 3297-3305. DOI: 10.1039/B508541A.

(86) Grimme, S.; Ehrlich, S.; Goerigk, L. Effect of the damping function in dispersion corrected density functional theory. *J. Comp. Chem.* **2011**, *32* (7), 1456-1465. DOI: https://doi.org/10.1002/jcc.21759.

(87) Grimme, S.; Antony, J.; Ehrlich, S.; Krieg, H. A consistent and accurate ab initio parametrization of density functional dispersion correction (DFT-D) for the 94 elements H-Pu. *J. Chem. Phys.* **2010**, *132* (15), 154104. DOI: 10.1063/1.3382344.

(88) Neese, F.; Wennmohs, F.; Hansen, A.; Becker, U. Efficient, approximate and parallel Hartree–Fock and hybrid DFT calculations. A 'chain-of-spheres' algorithm for the Hartree–Fock exchange. *Chem. Phys.* **2009**, *356* (1), 98-109. DOI: 10.1016/j.chemphys.2008.10.036.

(89) Weigend, F. Accurate Coulomb-Fitting Basis Sets for H to Rn. *Phys. Chem. Chem. Phys.* **2006**, *8* (9), 1057-1065. DOI: 10.1039/B515623H.

(90) Yanai, T.; Tew, D. P.; Handy, N. C. A New Hybrid Exchange–Correlation Functional using the Coulomb-Attenuating Method (CAM-B3LYP). *Chem. Phys. Lett.* **2004**, *393* (1), 51-57. DOI: 10.1016/j.cplett.2004.06.011.

(91) Chai, J.-D.; Head-Gordon, M. Long-range corrected hybrid density functionals with damped atom–atom dispersion corrections. *Phys. Chem. Chem. Phys.* **2008**, *10* (44), 6615-6620. DOI: 10.1039/B810189B.

(92) Humphrey, W.; Dalke, A.; Schulten, K. VMD: Visual molecular dynamics. *J. Mol. Graphics* **1996**, *14* (1), 33-38. DOI: 10.1016/0263-7855(96)00018-5.

(93) Zheng, J.; Xu, X.; Truhlar, D. G. Minimally augmented Karlsruhe basis sets. *Theor. Chem. Acc.* **2011**, *128* (3), 295-305. DOI: 10.1007/s00214-010-0846-z.

(94) Franzke, Y. J.; Holzer, C.; Andersen, J. H.; Begušić, T.; Bruder, F.; Coriani, S.; Della Sala, F.; Fabiano, E.; Fedotov, D. A.; Fürst, S.; et al. TURBOMOLE: Today and Tomorrow. *J. Chem. Theory Comput.* **2023**, *19* (20), 6859-6890. DOI: 10.1021/acs.jctc.3c00347.

(95) Perdew, J. P.; Burke, K.; Ernzerhof, M. Generalized Gradient Approximation Made Simple. *Phys. Rev. Lett.* **1996**, *77* (18), 3865-3868. DOI: 10.1103/PhysRevLett.77.3865.

(96) Adamo, C.; Barone, V. Toward Reliable Density Functional Methods without Adjustable Parameters: The PBE0 Model. *J. Chem. Phys.* **1999**, *110* (13), 6158-6170. DOI: 10.1063/1.478522.

(97) Henschel, H.; Andersson, A. T.; Jespers, W.; Mehdi Ghahremanpour, M.; van der Spoel, D. Theoretical Infrared Spectra: Quantitative Similarity Measures and Force Fields. *J. Chem. Theory Comput.* **2020**, *16* (5), 3307-3315. DOI: 10.1021/acs.jctc.0c00126.

(98) Skvortsov, D. S.; Vilesov, A. F. Using He Droplets for Measurements of Interconversion Enthalpy of Conformers in 2-Chloroethanol. *J. Chem. Phys.* **2009**, *130* (15), 151101. DOI: 10.1063/1.3111969.

(99) Leavitt, C. M.; Moore, K. B.; Raston, P. L.; Agarwal, J.; Moody, G. H.; Shirley, C. C.; Schaefer, H. F.; Douberly, G. E. Liquid Hot NAGMA Cooled to 0.4 K: Benchmark Thermochemistry of a Gas-Phase Peptide. *J. Phys. Chem. A* **2014**, *118* (41), 9692-9700. DOI: 10.1021/jp5092653.

(100) Thomas, D. A.; Chang, R.; Mucha, E.; Lettow, M.; Greis, K.; Gewinner, S.; Schöllkopf, W.; Meijer, G.; von Helden, G. Probing the conformational landscape and thermochemistry of DNA dinucleotide anions via helium nanodroplet infrared action spectroscopy. *Phys. Chem. Chem. Phys.* **2020**, *22* (33), 18400-18413. DOI: 10.1039/D0CP02482A.

(101) Harrilal, C. P.; DeBlase, A. F.; Fischer, J. L.; Lawler, J. T.; McLuckey, S. A.; Zwier, T. S. Infrared Population Transfer Spectroscopy of Cryo-Cooled Ions: Quantitative Tests of the Effects of Collisional Cooling on the Room Temperature Conformer Populations. *J. Phys. Chem. A* **2018**, *122* (8), 2096-2107. DOI: 10.1021/acs.jpca.7b12751.